STRESS CONCENTRATION AROUND A NANOVOID
ECCENTRICALLY EMBEDDED IN AN ELASTIC LAMINA
SUBJECTED TO FAR-FIELD LOADING

Changwen Mi

msp

STRESS CONCENTRATION AROUND A NANOVOID ECCENTRICALLY EMBEDDED IN AN ELASTIC LAMINA SUBJECTED TO FAR-FIELD LOADING

CHANGWEN MI

Stress concentration is one of the major challenges threatening the health and integrity of engineering structures. This paper analyzes the stress distributions around a spherical nanovoid near two parallel free surfaces. The loading is all-around uniform tension at infinity, perpendicular to the axis of symmetry of the infinite strip. Both plane surfaces of the strip assume traction free boundary conditions whereas the spherical void surface is modeled as a mathematical thin-film of Gurtin and Murdoch type. The method of Boussinesq's displacement functions is used in the analysis and the solutions are expressed semianalytically in terms of infinite series of Legendre functions and improper integrals involving Bessel functions. Numerical calculations are performed to illustrate the dependence of elastic fields on surface material properties, model size, void radius, and eccentricity. The results suggest the likelihood of optimizing stress concentrations in metallic materials and structures by the proper design of surface material properties, particularly of the residual surface stress.

1. Introduction

The presence of geometric defects such as holes, pits, and voids in elastic materials has received extensive investigation in literature because of the negative impact of stress concentrations on the integrity of engineering structures [Mura 1987]. Stress concentrations around spherically shaped voids have been one focus of micromechanics for decades, due probably to the relative simplicity in mathematical formulations. Most of these studies, however, have been concerned with spherical voids at the microscale [Tsuchida and Nakahara 1970; 1972; 1974; 1976; Tsuchida et al. 1976; Boccardo et al. 2015]. At such a length scale, stress concentration factors are typically independent of void radius provided that no additional characteristic lengths are involved. For models containing more than one characteristic length, stress concentrations typically depend on their ratios, instead of on individual length scale parameters.

Nonetheless, situations become more complicated as the characteristic length scales decrease to the nanoscale. As summarized in recent review articles on mechanics of nanostructured materials, surface effects dominate the mechanics and physics at small scales by introducing additional length scales [Duan et al. 2009; Wang et al. 2011; Chen and Yao 2014; Mi and Kouris 2014]. Stress distributions show strong dependence on void size. Several studies have been concerned with stress distributions around nanovoids embedded in an infinitely extended medium. By integrating traditionally excluded surface/interface energies and stresses into the classical Eshelby formalism for embedded inclusions, Sharma and Ganti [2004] first examined the size-dependent stress concentrations on the surface of a nanovoid. He and Li [2006] investigated the influence of surface mechanics on stress concentrations near a spherical void embedded in an infinite medium subjected to unidirectional remote load. Li et al. [2006] further solved the stress

Keywords: stress concentration, surface mechanics, elastic lamina, size dependence, displacement function method.

concentration factors around a spherical nanovoid under a few combinations of biaxial uniform loads. Duan et al. [2009] calculated the stress concentration factors of a spherical nanovoid by supplementing the equations of classical theory of elasticity with generalized Young–Laplace equations of surface elasticity.

More often than not, voids are found near a free surface. Therefore, displacements and stresses are additionally disturbed due to the presence of material boundaries. By the use of a displacement functions approach, Mi and Kouris [2013] examined the stress distributions around a nanosized void near a single free surface. More recently, they further evaluated the stress concentration factors due to a nanovoid equally close to two parallel free surfaces [Mi and Kouris 2015]. In both studies, a unidirectional uniform load applied at infinity was considered. Stress concentrations due to other loading conditions are also under development. For example, Mi et al. [2016] calculated elastic fields near a hemispherical pit at the plane boundary of an elastic half-space subjected to statically equivalent shear tractions.

Here we examine the stress concentrations around a nanosized void embedded at an arbitrary position in an infinite lamina of finite thickness. An all-around tensile stress field applied at the remote boundary of the lamina is considered. In view of the symmetry in both geometry and loading, the classical method of Boussinesq displacement functions is employed [Barber 2010] to solve the three-dimensional elastic problem. In the absence of body forces and torsional loads, two harmonic functions are sufficient to provide a general solution to the displacement equations of equilibrium. However, multiple sets of displacement functions are needed due to the disturbances caused by void and dual plane boundaries. For example, the voided lamina can be treated as the common domain belonging to both a voided infinite space and a defects-free lamina. For these domains, forms of (harmonic) displacement functions are well-known.

Based on this reasoning, a general solution was constructed by superposing a few groups of displacement functions, expressed in either spherical or cylindrical coordinates. Cylindrical and spherical harmonics are in the forms of improper integrals and infinite series, respectively. Consequently, they carry either continuous or discrete unknowns, in order to make the representations general enough. Although mathematically tedious and difficult, the subsequent solution principle is straightforward. Unknown functions in cylindrical harmonics were first expressed in terms of the unknown coefficients in spherical harmonics by imposing traction-free boundary conditions at both the upper and lower surfaces of the lamina.

Next, the Gurtin and Murdoch [1978] continuum model of surface mechanics was adopted to simulate the mechanical response of the void surface. In essence, this model treats a solid surface as a mathematical layer of vanishing thickness. On such a two-dimensional domain, both surface strain and surface stress were defined and thus a surface constitutive law was proposed. Finally, surface mechanics participates in the mechanics and physics of the problem by modifying the force balance condition across the surface. The enforcement of the modified boundary conditions at the void surface, by the use of a system of truncated infinite series involving Legendre polynomials, renders us the unknown coefficients in the spherical harmonics, and thus the unknown functions in cylindrical harmonics too. As the stresses due to the disturbance of plane boundaries are improper integrals of Howland type involving Bessel functions and hyperbolic functions, special algorithms were adopted to ensure the convergence and accuracy of their evaluations [Ling 1957; 1978; Ling and Lin 1971; Ling and Wu 1982].

It is worth mentioning that in the present study only the surface mechanics at the void surface is considered. Those at both plane boundaries are ignored, due to their secondary importance. As pointed out in [Mi and Kouris 2006], surface effects at flat surfaces may be neglected when those at one or more curved boundaries with finite radii of curvature are taken into account.

In terms of semianalytical series and integral expressions for stresses, extensive numerical calculations have been performed for various combinations of surface material properties, model size, void radius, and eccentricity. The results of the nanovoid symmetrically embedded in an elastic lamina and in an infinite medium have been reproduced as special cases of the eccentric model. Special consideration has been given to the determination of stress distributions in the immediate vicinity of the void due to far-field tension, since the disturbance of geometric defects is a short-range force field [Mura 1987]. The combined analytical and numerical analyses show that the stress concentration factors along the void surface can differ drastically from their classical counterparts. It is therefore possible to optimize the stress distributions by controlling the surface material properties of the void surface. At the nanoscale, the proper control of stresses and strains is a crucial factor in self-organized growth of quantum-dot crystals [Springholz et al. 1998].

The remainder of this paper is organized as follows. In Section 2 we outline in detail the mathematical method of solution, supplemented by three Appendices documenting indispensable yet tedious components of the solution procedure. Section 3 numerically examines the impact of surface material properties, model size, void radius, and eccentricity on the elastic fields in the vicinity of the embedded nanovoid. Finally, in Section 4, conclusions are drawn.

2. Method of solution

Consider a spherical nanovoid near either plane boundary of an infinite strip of finite thickness, as shown in Figure 1. Biaxial uniform boundary loads are applied at infinity, along directions parallel to both free surfaces. Given the geometry, cylindrical (r, θ, z) and spherical (R, φ, θ) coordinates will be used alternatively in the subsequent development. The transformation rules among these coordinates and the Cartesian one are also illustrated in Figure 1. The shear modulus G and Poisson's ratio ν are selected
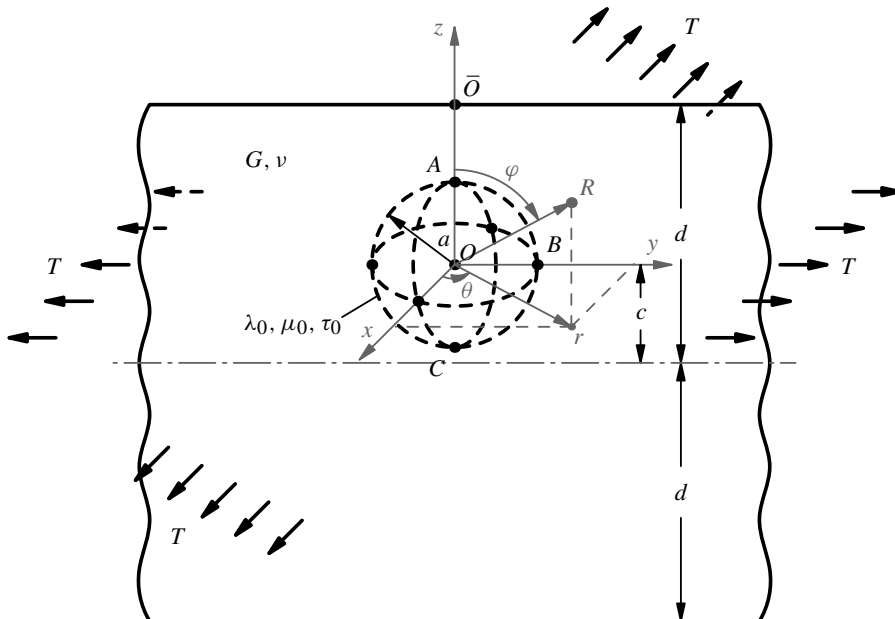

Figure 1. Geometry of the problem.

to represent the bulk material properties of the elastic lamina. Within the framework of the classical theory of micromechanics, three characteristic lengths exist in this problem, i.e., the half-thickness of the substrate d, void radius a, and the eccentricity c. Following [Gurtin and Murdoch 1978], three surface constants are required to fully accommodate the mechanical response of the void surface. Among them, τ_0 denotes residual surface stress whereas λ_0 and μ_0 are surface counterparts of Lamé constants. These surface material properties introduce a few more intrinsic length scales into the problem and thus make the solution more difficult to tackle.

In the absence of body forces, the axially symmetric equations of equilibrium in terms of displacements are given by

$$
\frac{\partial^2 u_r}{\partial z^2} + \frac{2(1-\nu)}{(1-2\nu)} \left\{ \frac{\partial^2 u_r}{\partial r^2} + \frac{1}{r} \frac{\partial u_r}{\partial r} - \frac{u_r}{r^2} \right\} + \frac{1}{(1-2\nu)} \frac{\partial^2 u_z}{\partial r \partial z} = 0,
$$
$$
\frac{\partial^2 u_z}{\partial r^2} + \frac{1}{r} \frac{\partial u_z}{\partial r} + \frac{2(1-\nu)}{(1-2\nu)} \frac{\partial^2 u_z}{\partial z^2} + \frac{1}{(1-2\nu)} \left\{ \frac{1}{r} \frac{\partial u_r}{\partial z} + \frac{\partial^2 u_r}{\partial r \partial z} \right\} = 0.
\tag{1}
$$

Thanks to the axial symmetry, two arbitrary harmonic functions (i.e., ϕ_0 and ϕ_3) are sufficient to yield the solution

$$
2G u_r = \frac{\partial \phi_0}{\partial r} + z \frac{\partial \phi_3}{\partial r}, \quad 2G u_z = \frac{\partial \phi_0}{\partial z} + z \frac{\partial \phi_3}{\partial z} - (3 - 4\nu)\phi_3.
\tag{2}
$$

Such a simple combination was first proposed by Boussinesq and is a special case of the more general Papkovich–Neuber representation [Barber 2010]. With the help of strain-displacement relationship and Hooke's law, the corresponding stresses read

$$
\sigma_{rr} = \frac{\partial^2 \phi_0}{\partial r^2} - \frac{z}{r} \frac{\partial \phi_3}{\partial r} - 2\nu \frac{\partial \phi_3}{\partial z} - z \frac{\partial^2 \phi_3}{\partial z^2}, \quad \sigma_{\theta\theta} = \frac{1}{r} \frac{\partial \phi_0}{\partial r} + \frac{z}{r} \frac{\partial \phi_3}{\partial r} - 2\nu \frac{\partial \phi_3}{\partial z},
$$
$$
\sigma_{zz} = \frac{\partial^2 \phi_0}{\partial z^2} - 2(1-\nu) \frac{\partial \phi_3}{\partial z} + z \frac{\partial^2 \phi_3}{\partial z^2}, \quad \sigma_{zr} = \frac{\partial^2 \phi_0}{\partial r \partial z} - (1-2\nu) \frac{\partial \phi_3}{\partial r} + z \frac{\partial^2 \phi_3}{\partial r \partial z}.
\tag{3}
$$

Spherical displacements and stresses are readily derived by using the relations

$$
\frac{\partial}{\partial r} = \sin\varphi \frac{\partial}{\partial R} + \frac{\cos\varphi}{R} \frac{\partial}{\partial \varphi}, \quad \frac{\partial}{\partial z} = \cos\varphi \frac{\partial}{\partial R} - \frac{\sin\varphi}{R} \frac{\partial}{\partial \varphi},
\tag{4}
$$

and the coordinate transformation equations

$$
\boldsymbol{e}_R = \sin\varphi \, \boldsymbol{e}_r + \cos\varphi \, \boldsymbol{e}_z, \quad \boldsymbol{e}_\varphi = \cos\varphi \, \boldsymbol{e}_r - \sin\varphi \, \boldsymbol{e}_z.
\tag{5}
$$

Traction-free boundary conditions are imposed at both plane boundaries of the infinite strip:

$$
(\sigma_{zr})_{z=d-c} = (\sigma_{zz})_{z=d-c} = 0, \quad (\sigma_{zr})_{z=-d-c} = (\sigma_{zz})_{z=-d-c} = 0.
\tag{6}
$$

At infinity,

$$
(\sigma_{rr})_{r\to\infty} = (\sigma_{\theta\theta})_{r\to\infty} = T.
\tag{7}
$$

As mentioned before, the mechanical response of the void surface is modeled by the theory of surface mechanics proposed in [Gurtin and Murdoch 1978]. In this context, the surface of the spherical void is treated as a mathematical film of vanishing thickness. The key component of the model lies in the

fact that at submicro- to nanoscales, the net traction across a solid surface is balanced by the surface divergence of surface stress ($\nabla_S \cdot \mathbf{\Sigma}$):

$$\sigma_{ij} n_j - T_i^{(n)} = (\nabla_S \cdot \mathbf{\Sigma})_i, \tag{8}$$

where n_i are components of the outward unit normal to the surface under consideration and $T_i^{(\mathbf{n})}$ of the external traction load, which is absent in the present case. The surface stress $\mathbf{\Sigma}$ is connected to the displacement gradient, evaluated at the surface, by the relations

$$\Sigma_{\alpha\beta} = \tau_0 \delta_{\alpha\beta} + (\mu_0 - \tau_0)(u_{\alpha,\beta} + u_{\beta,\alpha}) + (\lambda_0 + \tau_0) u_{\gamma,\gamma} \delta_{\alpha\beta} + \tau_0 u_{\alpha,\beta}, \quad \Sigma_{3\alpha} = \tau_0 u_{3,\alpha}. \tag{9}$$

Applying (8) and (9) to the geometry of the present problem, the boundary conditions at the void surface ($R = a$) can be expressed in spherical coordinates by

$$
\begin{aligned}
-\sigma_{RR} = (\nabla_S \cdot \Sigma)_R = {}& -\frac{2\tau_0}{R} - \frac{2(\lambda_0 + \mu_0)}{R^2}\left\{ 2u_R + \frac{\partial u_\varphi}{\partial \varphi} + \frac{\cos\varphi}{\sin\varphi} u_\varphi \right\} \\
& -\frac{\tau_0}{R^2}\left\{ 2u_R + 2\frac{\partial u_\varphi}{\partial \varphi} + \frac{2\cos\varphi}{\sin\varphi} u_\varphi - \frac{\partial^2 u_R}{\partial \varphi^2} - \frac{\cos\varphi}{\sin\varphi}\frac{\partial u_R}{\partial \varphi} \right\}, \\
-\sigma_{R\varphi} = (\nabla_S \cdot \Sigma)_\varphi = {}& \frac{\lambda_0}{R^2}\left\{ 2\frac{\partial u_R}{\partial \varphi} + \frac{\partial^2 u_\varphi}{\partial \varphi^2} + \frac{\cos\varphi}{\sin\varphi}\frac{\partial u_\varphi}{\partial \varphi} - \frac{u_\varphi}{\sin^2\varphi} \right\} \\
& + \frac{\mu_0}{R^2}\left\{ 2\frac{\partial u_R}{\partial \varphi} + 2\frac{\partial^2 u_\varphi}{\partial \varphi^2} + \frac{2\cos\varphi}{\sin\varphi}\frac{\partial u_\varphi}{\partial \varphi} - \frac{2\cos^2\varphi}{\sin^2\varphi} u_\varphi \right\} + \frac{2\tau_0}{R^2}\left\{ \frac{\partial u_R}{\partial \varphi} - u_\varphi \right\}.
\end{aligned}
\tag{10}
$$

For more details on Gurtin and Murdoch's model of surface mechanics, readers are invited to refer to their original publications [Gurtin and Murdoch 1975; 1978] and applications of the model [Benveniste 2006; Huang and Wang 2013; Mi and Kouris 2014].

To develop a solution to the present problem, forms of the two harmonic functions must be determined in advance. A few groups of displacement functions are proposed to construct the solution, the first of which is

$$\phi_0 = \frac{1-\nu}{2(1+\nu)}(r^2 - 2z^2)T, \quad \phi_3 = -\frac{z}{(1+\nu)}T. \tag{11}$$

In view of (3), this set corresponds to the applied load at infinity, $\sigma_{rr} = \sigma_{\theta\theta} = T$. The far-field boundary conditions in (7) are thus identically satisfied. Additional groups of displacement functions accommodating the disturbed elastic fields due to the presence of void and plane boundaries are also required. Let us first consider the disturbance caused by the void. In view of the solution to the harmonic equation defined outside of a sphere of radius a, we may try

$$\phi_0 = T \sum_{n=0}^{\infty} A_n \frac{d^{n+3}}{R^{n+1}} P_n[\mu], \quad \phi_3 = T \sum_{n=0}^{\infty} B_n \frac{d^{n+2}}{R^{n+1}} P_n[\mu], \tag{12}$$

where $P_n[\mu]$ denote Legendre functions of the first kind of order n and $\mu = \cos\varphi$. These functions were normalized with respect to the half-thickness d and the far-field tension T to make the unknown coefficients (A_n and B_n) dimensionless. Two additional sets of displacement functions are necessary to

accommodate the nature of finite thickness of the infinite strip:

$$\phi_0 = T \int_0^\infty \psi_1[\lambda] J_0[\lambda r] \cosh[\lambda z] \, d\lambda, \quad \phi_3 = T \int_0^\infty \lambda \psi_2[\lambda] J_0[\lambda r] \sinh[\lambda z] \, d\lambda; \tag{13}$$

$$\phi_0 = T \int_0^\infty \overline{\psi}_1[\lambda] J_0[\lambda r] \sinh[\lambda z] \, d\lambda, \quad \phi_3 = T \int_0^\infty \lambda \overline{\psi}_2[\lambda] J_0[\lambda r] \cosh[\lambda z] \, d\lambda, \tag{14}$$

where $J_0[\lambda r]$ is a Bessel function of the first kind of zeroth order and $\psi_1[\lambda]$, $\psi_2[\lambda]$, $\overline{\psi}_1[\lambda]$ and $\overline{\psi}_2[\lambda]$ are unknown functions of the integral variable, to be determined by satisfying the boundary conditions in (6). The displacement functions (13) and (14) represent the symmetric and antisymmetric components of the disturbance due to both free surfaces, respectively.

The displacement functions in (12) are expressed in spherical coordinates. In order to satisfy the boundary conditions at the plane boundaries in (6), they need be transformed into cylindrical coordinates. From [Gradshteyn and Ryzhik 2014], an integral representation of the azimuthally independent spherical harmonics can be found for the half-space $z > 0$:

$$\frac{P_n[\mu]}{R^{n+1}} = \frac{1}{n!} \int_0^\infty \lambda^n J_0[\lambda r] e^{-\lambda z} \, d\lambda. \tag{15}$$

The displacement functions in (12) can therefore be transformed to

$$\phi_0 = T \int_0^\infty \left\{ \sum_{n=0}^\infty \frac{A_n d^{n+3} \lambda^n}{n!} \right\} J_0[\lambda r] e^{-\lambda z} \, d\lambda,$$

$$\phi_3 = T \int_0^\infty \lambda \left\{ \sum_{n=0}^\infty \frac{B_n d^{n+2} \lambda^{n-1}}{n!} \right\} J_0[\lambda r] e^{-\lambda z} \, d\lambda. \tag{16}$$

Replacing (z) with $(-z)$, (μ) with $(-\mu)$, and employing the parity property of the Legendre function [Arfken et al. 2013], it can be found that for $z < 0$,

$$\frac{P_n[\mu]}{R^{n+1}} = \frac{(-1)^n}{n!} \int_0^\infty \lambda^n J_0[\lambda r] e^{\lambda z} \, d\lambda. \tag{17}$$

Then, the displacement functions in (12) become

$$\phi_0 = T \int_0^\infty \left\{ \sum_{n=0}^\infty \frac{(-1)^n A_n d^{n+3} \lambda^n}{n!} \right\} J_0[\lambda r] e^{\lambda z} \, d\lambda,$$

$$\phi_3 = T \int_0^\infty \lambda \left\{ \sum_{n=0}^\infty \frac{(-1)^n B_n d^{n+2} \lambda^{n-1}}{n!} \right\} J_0[\lambda r] e^{\lambda z} \, d\lambda, \tag{18}$$

At this point, the expressions for stresses at the upper surface of the strip can be developed by the superposition of the displacement functions (13), (14), and (16). Those at the lower surface are derived from (13), (14), and (18). The enforcement of the plane boundary conditions in (6) yields the following relations:

$$\psi_1 = \sum_{n=0}^\infty \frac{A_{2n}(d\lambda)^{2n+3}}{2(2n)!} \left\{ (3 - 4v)(K^+ - I^-) + L^+ - N^- + 2d\lambda \left(I^- + \frac{c}{d} J^+ - K^+ \right) \right\}$$

$$+ \sum_{n=0}^{\infty} \frac{A_{2n+1}(d\lambda)^{2n+4}}{2(2n+1)!} \left\{ (3-4\nu)J^+ - M^- + 2d\lambda \left(\frac{c}{d}I^- + \frac{c}{d}K^+ - J^+ \right) \right\}$$

$$+ \sum_{n=0}^{\infty} \frac{B_{2n}(d\lambda)^{2n+2}}{(2n)!} \left\{ 2(1-\nu)(1-2\nu)J^+ + c\lambda((3-4\nu)I^- + N^-) \right. \tag{19}$$

$$\left. + d^2\lambda^2 \left(\frac{2c}{d}K^+ - \left(1 + \frac{c^2}{d^2} \right)J^+ \right) \right\}$$

$$+ \sum_{n=0}^{\infty} \frac{B_{2n+1}(d\lambda)^{2n+3}}{(2n+1)!} \left\{ 2(1-\nu)(1-2\nu)(K^+ - I^-) + c\lambda M^- \right.$$

$$\left. + d^2\lambda^2 \left(\frac{2c}{d}J^+ - \left(1 + \frac{c^2}{d^2} \right)K^+ + \left(1 - \frac{c^2}{d^2} \right)I^- \right) \right\},$$

$$\overline{\psi}_1 = \sum_{n=0}^{\infty} \frac{A_{2n}(d\lambda)^{2n+3}}{2(2n)!} \left\{ (3-4\nu)J^+ - M^- + 2d\lambda \left(\frac{c}{d}(K^+ - I^-) - J^+ \right) \right\}$$

$$+ \sum_{n=0}^{\infty} \frac{A_{2n+1}(d\lambda)^{2n+4}}{2(2n+1)!} \left\{ (3-4\nu)(K^+ + I^-) - L^+ - N^- + 2d\lambda \left(\frac{c}{d}J^+ - K^+ - I^- \right) \right\}$$

$$+ \sum_{n=0}^{\infty} \frac{B_{2n}(d\lambda)^{2n+2}}{(2n)!} \left\{ 2(1-\nu)(1-2\nu)(K^+ + I^-) + c\lambda M^- \right. \tag{20}$$

$$\left. + d^2\lambda^2 \left(\frac{2c}{d}J^+ - \left(1 - \frac{c^2}{d^2} \right)I^- - \left(1 + \frac{c^2}{d^2} \right)K^+ \right) \right\}$$

$$+ \sum_{n=0}^{\infty} \frac{B_{2n+1}(d\lambda)^{2n+3}}{(2n+1)!} \left\{ 2(1-\nu)(1-2\nu)J^+ + c\lambda(N^- - (3-4\nu)I^-) \right.$$

$$\left. + d^2\lambda^2 \left(\frac{2c}{d}K^+ - \left(1 + \frac{c^2}{d^2} \right)J^+ \right) \right\},$$

$$\psi_2 = \sum_{n=0}^{\infty} \frac{A_{2n}(d\lambda)^{2n+3}}{(2n)!}(K^+ - I^-) + \sum_{n=0}^{\infty} \frac{A_{2n+1}(d\lambda)^{2n+4}}{(2n+1)!}J^+$$

$$+ \sum_{n=0}^{\infty} \frac{B_{2n}(d\lambda)^{2n+2}}{2(2n)!} \left\{ (3-4\nu)J^+ + M^- + 2d\lambda \left(J^+ - \frac{c}{d}(K^+ - I^-) \right) \right\} \tag{21}$$

$$+ \sum_{n=0}^{\infty} \frac{B_{2n+1}(d\lambda)^{2n+3}}{2(2n+1)!} \left\{ (3-4\nu)(K^+ - I^-) - L^+ + N^- + 2d\lambda \left(K^+ - I^- - \frac{c}{d}J^+ \right) \right\},$$

$$\frac{\overline{\psi}_2}{d^3} = \sum_{n=0}^{\infty} \frac{A_{2n}(d\lambda)^{2n+3}}{(2n)!}J^+ + \sum_{n=0}^{\infty} \frac{A_{2n+1}(d\lambda)^{2n+4}}{(2n+1)!}(K^+ + I^-)$$

$$+ \sum_{n=0}^{\infty} \frac{B_{2n}(d\lambda)^{2n+2}}{2(2n)!} \left\{ (3-4\nu)(K^+ + I^-) + L^+ + N^- + 2d\lambda \left(K^+ + I^- - \frac{c}{d}J^+ \right) \right\} \tag{22}$$

$$+ \sum_{n=0}^{\infty} \frac{B_{2n+1}(d\lambda)^{2n+3}}{2(2n+1)!} \left\{ (3-4\nu)J^+ + M^- + 2d\lambda \left(J^+ - \frac{c}{d}(K^+ + I^-) \right) \right\},$$

where

$$I^{\pm} = \frac{1}{\sinh[2x] - 2x} \pm \frac{1}{\sinh[2x] + 2x}, \quad J^{\pm} = I^{\pm}\sinh[2cx/d], \quad K^{\pm} = I^{\pm}\cosh[2cx/d],$$
$$L^{\pm} = I^{\pm}e^{-2x}, \quad M^{\pm} = I^{\pm}e^{-2x}\sinh[2cx/d], \quad N^{\pm} = I^{\pm}e^{-2x}\cosh[2cx/d], \quad x = d\lambda. \tag{23}$$

Next, we impose the boundary conditions at the void surface $R = a$, given in (10). For this purpose, the displacement functions (13) and (14) must be transformed into spherical coordinates. With the help of the series representations of cylindrical harmonics [Gradshteyn and Ryzhik 2014],

$$J_0[\lambda r]\cosh\lambda z = \sum_{n=0}^{\infty}\frac{(\lambda R)^{2n}}{(2n)!}P_{2n}[\mu], \quad J_0[\lambda r]\sinh\lambda z = \sum_{n=0}^{\infty}\frac{(\lambda R)^{2n+1}}{(2n+1)!}P_{2n+1}[\mu]. \tag{24}$$

Equations (13) and (14) can be combined into a single group,

$$\phi_0 = T\sum_{n=0}^{\infty}\alpha_n\frac{R^n}{d^{n-2}}P_n[\mu], \quad \phi_3 = T\sum_{n=0}^{\infty}\beta_n\frac{R^n}{d^{n-1}}P_n[\mu], \tag{25}$$

where

$$\alpha_{2n} = d^{2n-2}\int_0^{\infty}\frac{\psi_1\lambda^{2n}}{(2n)!}\,d\lambda, \quad \alpha_{2n+1} = d^{2n-1}\int_0^{\infty}\frac{\overline{\psi}_1\lambda^{2n+1}}{(2n+1)!}\,d\lambda,$$
$$\beta_{2n} = d^{2n-1}\int_0^{\infty}\frac{\overline{\psi}_2\lambda^{2n+1}}{(2n)!}\,d\lambda, \quad \beta_{2n+1} = d^{2n}\int_0^{\infty}\frac{\psi_2\lambda^{2n+2}}{(2n+1)!}\,d\lambda. \tag{26}$$

Substituting (19)–(22) into (26), we obtain

$$\alpha_{2n} = \sum_{m=0}^{\infty}A_{2m}q_{2m}^{2n}\left\{(3-4\nu)(K_{2m+2n}^+ - I_{2m+2n}^-) + L_{2m+2n}^+ - N_{2m+2n}^- \right.$$
$$\left. + (2m+2n+1)\left(\frac{c}{d}J_{2m+2n+1}^+ - K_{2m+2n+1}^+ + I_{2m+2n+1}^-\right)\right\}$$

$$+ \sum_{m=0}^{\infty}A_{2m+1}q_{2m+1}^{2n}\left\{(3-4\nu)J_{2m+2n+1}^+ - M_{2m+2n+1}^- \right.$$
$$\left. + (2m+2n+2)\left(\frac{c}{d}K_{2m+2n+2}^+ + \frac{c}{d}I_{2m+2n+2}^- - J_{2m+2n+2}^+\right)\right\}$$

$$+ 2\sum_{m=0}^{\infty}B_{2m}q_{2m}^{2n}\left\{\frac{4(1-\nu)(1-2\nu)}{(2m+2n)}J_{2m+2n-1}^+ + \frac{c}{d}((3-4\nu)I_{2m+2n}^- + N_{2m+2n}^-) \right. \tag{27}$$
$$\left. + (2m+2n+1)\left(\frac{c}{d}K_{2m+2n+1}^+ - \frac{1}{2}\left(1+\frac{c^2}{d^2}\right)J_{2m+2n+1}^+\right)\right\}$$

$$+ 2\sum_{m=0}^{\infty}B_{2m+1}q_{2m+1}^{2n}\left\{\frac{4(1-\nu)(1-2\nu)}{(2m+2n+1)}(K_{2m+2n}^+ - I_{2m+2n}^-) \right.$$
$$+ (2m+2n+2)\frac{c}{d}J_{2m+2n+2}^+ + \frac{c}{d}M_{2m+2n+1}^-$$
$$\left. + (m+n+1)\left(\left(1-\frac{c^2}{d^2}\right)I_{2m+2n+2}^- - \left(1+\frac{c^2}{d^2}\right)K_{2m+2n+2}^+\right)\right\},$$

$$
\begin{aligned}
\alpha_{2n+1} = &\sum_{m=0}^{\infty} A_{2m} q_{2m}^{2n+1} \Bigg\{ (3-4v) J_{2m+2n+1}^{+} - M_{2m+2n+1}^{-} \\
&\qquad\qquad + (2m+2n+2)\Big(\frac{c}{d} K_{2m+2n+2}^{+} - \frac{c}{d} I_{2m+2n+2}^{-} - J_{2m+2n+2}^{+} \Big) \Bigg\} \\
&+ \sum_{m=0}^{\infty} A_{2m+1} q_{2m+1}^{2n+1} \Bigg\{ (3-4v)(K_{2m+2n+2}^{+} + I_{2m+2n+2}^{-}) - L_{2m+2n+2}^{+} - N_{2m+2n+2}^{-} \\
&\qquad\qquad + (2m+2n+3)\Big(\frac{c}{d} J_{2m+2n+3}^{+} - K_{2m+2n+3}^{+} - I_{2m+2n+3}^{-} \Big) \Bigg\} \\
&+ 2\sum_{m=0}^{\infty} B_{2m} q_{2m}^{2n+1} \Bigg\{ \frac{4(1-v)(1-2v)}{(2m+2n+1)} (K_{2m+2n}^{+} + I_{2m+2n}^{-}) \\
&\qquad\qquad + (2m+2n+2)\frac{c}{d} J_{2m+2n+2}^{+} + \frac{c}{d} M_{2m+2n+1}^{-} \\
&\qquad\qquad - (m+n+1)\Big(\Big(1 - \frac{c^2}{d^2}\Big) I_{2m+2n+2}^{-} + \Big(1 + \frac{c^2}{d^2}\Big) K_{2m+2n+2}^{+} \Big) \Bigg\} \\
&+ 2\sum_{m=0}^{\infty} B_{2m+1} q_{2m+1}^{2n+1} \Bigg\{ \frac{4(1-v)(1-2v)}{(2m+2n+2)} J_{2m+2n+1}^{+} + \frac{c}{d}(N_{2m+2n+2}^{-} - (3-4v) I_{2m+2n+2}^{-}) \\
&\qquad\qquad + (2m+2n+3)\Big(\frac{c}{d} K_{2m+2n+3}^{+} - \frac{1}{2}\Big(1 + \frac{c^2}{d^2}\Big) J_{2m+2n+3}^{+} \Big) \Bigg\},
\end{aligned}
\tag{28}
$$

$$
\begin{aligned}
\beta_{2n} = &\sum_{m=0}^{\infty} A_{2m} q_{2m}^{2n} (2m+2n+1) J_{2m+2n+1}^{+} \\
&+ \sum_{m=0}^{\infty} A_{2m+1} q_{2m+1}^{2n} (2m+2n+2) \{ K_{2m+2n+2}^{+} + I_{2m+2n+2}^{-} \} \\
&+ \sum_{m=0}^{\infty} B_{2m} q_{2m}^{2n} \Bigg\{ (3-4v)(K_{2m+2n}^{+} + I_{2m+2n}^{-}) + L_{2m+2n}^{+} + N_{2m+2n}^{-} \\
&\qquad\qquad + (2m+2n+1)\Big(K_{2m+2n+1}^{+} + I_{2m+2n+1}^{-} - \frac{c}{d} J_{2m+2n+1}^{+} \Big) \Bigg\} \\
&+ \sum_{m=0}^{\infty} B_{2m+1} q_{2m+1}^{2n} \Bigg\{ (3-4v) J_{2m+2n+1}^{+} + M_{2m+2n+1}^{-} \\
&\qquad\qquad + (2m+2n+2)\Big(J_{2m+2n+2}^{+} - \frac{c}{d}(K_{2m+2n+2}^{+} + I_{2m+2n+2}^{-}) \Big) \Bigg\},
\end{aligned}
\tag{29}
$$

$$
\begin{aligned}
\beta_{2n+1} = &\sum_{m=0}^{\infty} A_{2m} q_{2m}^{2n+1} (2m+2n+2) \{ K_{2m+2n+2}^{+} - I_{2m+2n+2}^{-} \} \\
&+ \sum_{m=0}^{\infty} A_{2m+1} q_{2m+1}^{2n+1} (2m+2n+3) J_{2m+2n+3}^{+} \\
&+ \sum_{m=0}^{\infty} B_{2m} q_{2m}^{2n+1} \Bigg\{ (3-4v) J_{2m+2n+1}^{+} + M_{2m+2n+1}^{-} \\
&\qquad\qquad + (2m+2n+2)\Big(J_{2m+2n+2}^{+} - \frac{c}{d}(K_{2m+2n+2}^{+} - I_{2m+2n+2}^{-}) \Big) \Bigg\}
\end{aligned}
\tag{30}
$$

$$+ \sum_{m=0}^{\infty} B_{2m+1} q_{2m+1}^{2n+1} \left\{ (3-4\nu)(K_{2m+2n+2}^+ - I_{2m+2n+2}^-) - L_{2m+2n+2}^+ + N_{2m+2n+2}^- \right.$$
$$\left. + (2m+2n+3)\left(K_{2m+2n+3}^+ - I_{2m+2n+3}^- - \frac{c}{d} J_{2m+2n+3}^+ \right) \right\},$$

where

$$q_m^n = \frac{(m+n)!}{m!n!2^{2m+n+1}}, \quad I_k^\pm = \frac{2^k}{k!} \int_0^\infty I^\pm x^k \, \mathrm{d}x, \quad J_k^\pm = \frac{2^k}{k!} \int_0^\infty I^\pm x^k \sinh[2cx/d] \, \mathrm{d}x,$$

$$K_k^\pm = \frac{2^k}{k!} \int_0^\infty I^\pm x^k \cosh[2cx/d] \, \mathrm{d}x, \qquad\qquad L_k^\pm = \frac{2^k}{k!} \int_0^\infty I^\pm e^{-2x} x^k \, \mathrm{d}x, \qquad (31)$$

$$M_k^\pm = \frac{2^k}{k!} \int_0^\infty I^\pm e^{-2x} x^k \sinh[2cx/d] \, \mathrm{d}x, \qquad N_k^\pm = \frac{2^k}{k!} \int_0^\infty I^\pm e^{-2x} x^k \cosh[2cx/d] \, \mathrm{d}x.$$

These integrals are known as *Howland type*. Their evaluations are nontrivial and separately documented in Appendix A.

Given the displacement functions (11), (12), and (25), both the stresses and the surface divergence of surface stresses at the void surface can be evaluated. The boundary conditions in (10) then become

$$\sum_{n=0}^{\infty} \left\{ \left(i_{SA1} + i_{A1} \frac{d^{n+3}}{a^{n+3}} \right) A_n + \left(i_{SB1} + i_{B1} \frac{d^{n+1}}{a^{n+1}} \right) B_{n-1} + \left(i_{SB2} + i_{B2} \frac{d^{n+3}}{a^{n+3}} \right) B_{n+1} \right.$$
$$\left. + \left(i_{S\alpha1} + i_{\alpha1} \frac{a^{n-2}}{d^{n-2}} \right) \alpha_n + \left(i_{S\beta1} + i_{\beta1} \frac{a^{n-2}}{d^{n-2}} \right) \beta_{n-1} + \left(i_{S\beta2} + i_{\beta2} \frac{a^n}{d^n} \right) \beta_{n+1} \right\} P_n[\mu]$$
$$= \left\{ \frac{2\tau_0}{aT} - \frac{2}{3} + \frac{2(1-2\nu)(2\lambda_0 + 2\mu_0 + \tau_0)}{3aG(1+\nu)} \right\} P_0[\mu] + \left\{ \frac{2}{3} + \frac{2(\lambda_0 + \mu_0 - \tau_0)}{3aG} \right\} P_2[\mu],$$
$$\sum_{n=1}^{\infty} \left\{ \left(l_{SA1} + l_{A1} \frac{d^{n+3}}{a^{n+3}} \right) A_n + \left(l_{SB1} + l_{B1} \frac{d^{n+1}}{a^{n+1}} \right) B_{n-1} + \left(l_{SB2} + l_{B2} \frac{d^{n+3}}{a^{n+3}} \right) B_{n+1} \right. \qquad (32)$$
$$\left. + \left(l_{S\alpha1} + l_{\alpha1} \frac{a^{n-2}}{d^{n-2}} \right) \alpha_n + \left(l_{S\beta1} + l_{\beta1} \frac{a^{n-2}}{d^{n-2}} \right) \beta_{n-1} + \left(l_{S\beta2} + l_{\beta2} \frac{a^n}{d^n} \right) \beta_{n+1} \right\} P_n'[\mu]$$
$$= \left\{ \frac{(\lambda_0 + 3\mu_0 - \tau_0)}{3aG} - \frac{1}{3} \right\} P_2'[\mu],$$

where i_{SA1}, i_{A1}, i_{SB1}, i_{B1}, i_{SB2}, i_{B2}, $i_{S\alpha1}$, $i_{\alpha1}$, $i_{S\beta1}$, $i_{\beta1}$, $i_{S\beta2}$, $i_{\beta2}$, l_{SA1}, l_{A1}, l_{SB1}, l_{B1}, l_{SB2}, l_{B2}, $l_{S\alpha1}$, $l_{\alpha1}$, $l_{S\beta1}$, $l_{\beta1}$, $l_{S\beta2}$, and $l_{\beta2}$ are all dimensionless functions of the order number n, void radius a, half-thickness d, shear modulus G, Poisson's ratio ν, and the three surface material constants. For brevity, their expressions are provided in Appendix B. Equating the coefficients of Legendre functions $P_n[\mu]$ and their derivatives $P_n'[\mu]$ lead to a system of linear equations for the unknown constants A_n and B_n. The solution is obtained by solving the linear system.

A careful examination of (32) and those coefficients defined in Appendix B reveals that the strength of the void surface is governed by four intrinsic dimensionless parameters: $\lambda_0' = \lambda_0/aG$, $\mu_0' = \mu_0/aG$, $\tau_0' = \tau_0/aG$, and $\tau_0'' = \tau_0/aT$. The impact of surface mechanics becomes significant when any of these parameters approaches the order of magnitude of unity, or at least to one tenth. For smaller magnitudes, the inclusion of the model of surface mechanics only brings negligible modifications to the classical

solution. By a combined analytical and numerical analysis, Mi and Kouris [2014] recently analyzed the relative importance of these four dimensionless quantities. For a metal system, the last of these four parameters ($\tau_0'' = \tau_0/aT$) dominates since the shear modulus of a metal is about two orders of magnitude higher than its yield strength. The other three parameters become relatively more important in models composed of soft materials such as gelatin gels and rubbers [Mi et al. 2016].

Subsequently, by the superposition of the expressions that can be developed from all displacement functions, all stresses and displacements can be calculated in both cylindrical and spherical coordinates. Nonetheless, difficulties arise when evaluating stresses due to the displacement functions (13) and (14). As can be seen from the expansions in (24), in spherical coordinates the displacement functions in (25) are valid solutions to the harmonic equation only in regions near the void. For regions far away from the void, both series diverge. As a result, the representations in (25) are most helpful to the enforcement of the boundary conditions at the void surface.

On the other hand, when directly evaluating stresses from (13) and (14), integrals involving more complicated integrands than those shown in (31) are encountered. They can be represented by 24 integrals of Howland type, possessing an additional Bessel function and a hyperbolic function in the integrands. The evaluations of these integrals require special consideration, which are presented in Appendix C.

3. Results and discussion

Several numerical experiments were performed when all-around tension at infinity was considered. The infinite strip is assumed to be an isotropic continuum made of nickel, whose shear modulus and Poisson's ratio are respectively $G = 76$ GPa and $\nu = 0.31$. The far-field tensile stress field was chosen so as to ensure that no yielding is resulted: $T = 100$ MPa. Stresses and displacements were calculated for various combinations of surface material properties, model size, eccentricity, and void radius.

Based on the dimension analysis presented at the end of last section, it is obvious that the effects of surface mechanics are both material and load dependent. For practical applications of the developed solution, the values of these four parameters and therefore the strength of surface mechanics must be informed from both the bulk and surface material properties of the given physical model. Even for crystalline metals, it is a primary challenge to determine accurate values for the residual surface stress and the two surface Lamé constants. Nonetheless, molecular simulations demonstrate that both the residual surface stress and the stiffness constants of a crystalline surface have a magnitude of about 1 N/m [Gumbsch and Daw 1991; Shenoy 2005; Mi et al. 2008], though either sign is possible. For a nanovoid of radius 10 nm, $\tau_0/a, \lambda_0/a, \mu_0/a \sim 100$ MPa, whose magnitude is reasonably close to the practical loads of most engineering materials. In view of this fact, we have based our calculations merely on several plain crystalline surfaces and two nominal models to investigate the physical significance of surface elasticity. These case studies are sufficiently representative.

3.1. *Convergence test.* It can be observed that the displacement functions (12) and (25) are complete and the convergence of the series is guaranteed. However, these displacement functions are in the form of infinite series. As a result, the fulfillment of boundary conditions results in an infinite set of simultaneous linear equations; see (32). It is not possible to analytically solve such an infinite system without truncation. We therefore must truncate the infinite series in (32) at a finite order N, which inevitably introduces numerical approximation to the solution.
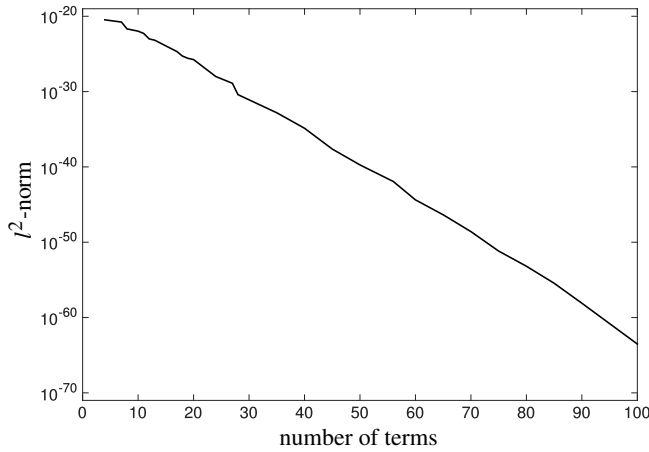
Figure 2. Variation of the l^2-norm of the error vector of the linear system (32) as a function of the number of terms included in the series after truncation.

In order to numerically test the convergence of the solution as a function of the number of terms kept in the truncated series, we computed the l^2-norm of the error vector of the linear system (32). The error vector is formed by the residuals of all linear equations after truncation. As a convention, the square root of the error vector is defined as the l^2-norm.

To evaluate numerically the semianalytical solution and analyze its sensitivity to the truncation parameter, we here take a quite general model as an example. The three characteristic lengths of the model were chosen as $d = 20$ nm, $a = 6$ nm, and $c = 10$ nm. In addition, we chose to model the void surface by the mechanical behavior of a crystalline copper surface whose normal is defined by the crystalline direction [111]. A pair of square brackets is often used to denote a crystalline direction in crystallography. In this analysis, values of the truncation that number up to 100 were considered. A semilogarithmic plot with the l^2-norm of the error vector is presented in Figure 2. It can be concluded from the plot that the l^2-norm decreases exponentially as the truncation number N increases. For both the classical and the modified solutions, no more than 20 terms are needed to satisfy the boundaries conditions at the void surface, with an accuracy up to five significant figures for displacements and stresses. We therefore assume the truncation number $N = 20$ from now on.

3.2. *Effects of surface material properties.* To investigate the influence of surface material properties, we first examined the stress disturbances caused by a nanovoid of radius 6 nm, eccentrically embedded ($c = 10$ nm) in an infinite strip with half-thickness $d = 20$ nm. In addition to the classical case ($\lambda_0 = \mu_0 = \tau_0 = 0$), six additional surface models were considered. The values of the three surface constants in these models were taken or designed on the basis of [Mi et al. 2008; Shenoy 2005]. For example, we chose to treat the void surface as a plain crystalline copper or nickel surface with two representative surface orientations in four surface models. In crystallography notation, a pair of parentheses is typically used to stand for a crystalline surface. For example, the combination (111) represents a crystalline surface with the crystalline direction [111] as its surface normal. In the remaining two models, we assigned simple nominal values to all three surface constants, i.e., $\lambda_0 = \mu_0 = \tau_0 = 1$ and $\lambda_0 = \mu_0 = \tau_0 = -1$. The rationale
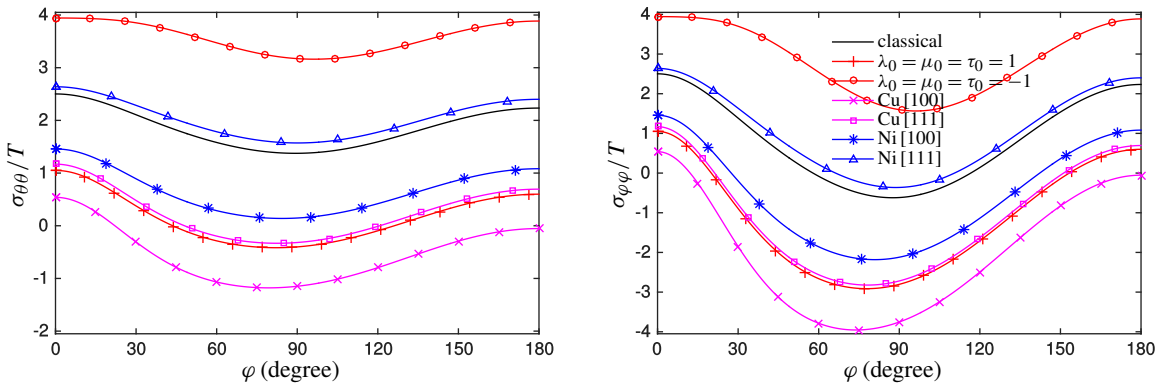
Figure 3. Distribution of hoop, left, and tangential stresses, right, along the void surface ($R = a$). Both subfigures consider six surface models, in addition to the classical solution. Three characteristic lengths of the model are chosen as: $d = 20\,\text{nm}$, $a = 0.3d$, and $c = 0.5d$.
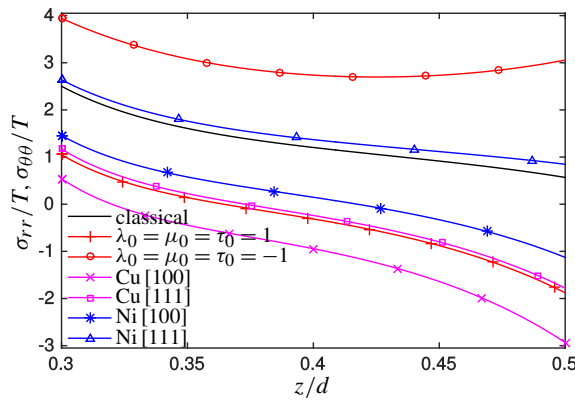

Figure 4. Variation of σ_{rr} and $\sigma_{\theta\theta}$ along the axis of symmetry ($a \leq z \leq d - c$) as a function of nondimensionalized coordinate z/d. In addition to the classical solution, six surface models are considered. Three characteristic lengths of the model are chosen as: $d = 20$ nm, $a = 0.3d$, and $c = 0.5d$.

behind such simple choices is as follows. Both experimental measurements [Cammarata 1994] and atomistic calculations [Mi et al. 2008; Shenoy 2005] have demonstrated that all surface elastic properties of a crystalline surface/interface are roughly in the order of magnitude 1 N/m. Their sign, surprisingly, can be either positive or negative. The possibility of negative surface constants, particularly of negative surface Lamé parameters, is out of expectation and has been extensively discussed [Cammarata 1994; Mi et al. 2008; Shenoy 2005].

Figure 3 shows the hoop ($\sigma_{\theta\theta}$) and tangential ($\sigma_{\varphi\varphi}$) stresses along the void surface $R = a$. For all surface models, stress concentration factors reach high tensile values at the north pole A of the void. The stress concentrations at the south pole C are slightly less severe, due to the eccentricity of the void. Low tensile/compressive values of the stress concentration factors were found near but not exactly on

the equator of the void, due again to the eccentricity of the void. It can be seen that stress distributions in the top half of the strip are more disturbed by the presence of infinite plane boundaries. For this reason, we further plotted both the cylindrical radial (σ_{rr}) and hoop ($\sigma_{\theta\theta}$) stresses along the positive z-axis, as shown in Figure 4. Along the symmetry axis, these two stress components are identical.

From the various cases shown in Figures 3 and 4, it is obvious that stress distributions depend strongly on particular models of surface mechanics. Ni (111) and one of the two nominal models ($\lambda_0 = \mu_0 = \tau_0 = -1$) resulted in more severe stress concentrations than the classical solution. The other four surface models help to reduce the stress concentrations. Among them, the nominal model ($\lambda_0 = \mu_0 = \tau_0 = -1$) and Cu (100) represent the worst and best scenarios, respectively. In the latter case, compressive hoop and tangential stresses were found in most regions of the void surface, except in the immediate vicinity of the void poles A and C. This is quite impressive, given the fact that the remote boundary loading is purely tensile.

Based on the previous dimension analysis on the four intrinsic dimensionless parameters for a metal system, the residual surface stress alone is far more important than surface elasticity. Consequently, it is reasonable to approximate the stresses around a nanovoid embedded in an infinite substrate subjected to all-around far-field tension by

$$
\begin{aligned}
\frac{\sigma_{RR}}{T} &= \frac{2\tau_0}{Ta}\frac{a^3}{R^3} + \frac{2}{3} - \frac{2}{3}\frac{a^3}{R^3} - \left\{\frac{2}{3} - \frac{10(5-\nu)}{3(7-5\nu)}\frac{a^3}{R^3} + \frac{12}{(7-5\nu)}\frac{a^5}{R^5}\right\}P_2[\mu], \\
\frac{\sigma_{\theta\theta}}{T} &= -\frac{\tau_0}{Ta}\frac{a^3}{R^3} + 1 + \frac{(4-5\nu)}{(7-5\nu)}\frac{a^3}{R^3} + \frac{1}{(7-5\nu)}\frac{a^5}{R^5} - \left\{\frac{5(1-2\nu)}{(7-5\nu)}\frac{a^3}{R^3} - \frac{5}{(7-5\nu)}\frac{a^5}{R^5}\right\}P_2[\mu], \qquad (33) \\
\frac{\sigma_{\varphi\varphi}}{T} &= -\frac{\tau_0}{Ta}\frac{a^3}{R^3} + \frac{1}{3} + \frac{(2+5\nu)}{3(7-5\nu)}\frac{a^3}{R^3} - \frac{1}{(7-5\nu)}\frac{a^5}{R^5} + \left\{\frac{2}{3} - \frac{5(1-2\nu)}{3(7-5\nu)}\frac{a^3}{R^3} + \frac{7}{(7-5\nu)}\frac{a^5}{R^5}\right\}P_2[\mu].
\end{aligned}
$$

The above solution is a simple superposition of the classical solution with the effects due to the residual surface stress alone. It now becomes obvious that for nanosized voids the first term in any stress component is in the same order of magnitude as the other ones and therefore must be taken into account. The dependence of stress distributions on surface models in Figures 3 and 4 can be qualitatively explained by (33). The values of residual surface stress are $\tau_0 = -1$, -0.11 (Ni (111)), 0 (classical), 0.7 (Ni (100)), 0.95 (Cu (111)), 1, and 1.41 N/m (Cu (100)) for the seven curves in each subfigure of Figures 3 and 4. The trend is very clear that stress distributions are significantly affected by the value of the residual surface stress. Positive values of τ_0 help to reduce stress levels whereas the negative ones tend to intensify the stress concentrations. For compressive far-field loading, the conclusions should obviously be reversed. It should also be noted that (33) cannot be used to quantitatively predict the curves in Figures 3 and 4. The errors represent the disturbances introduced by both the top and bottom plane boundaries.

3.3. Effects of model size.

Because the impact of surface mechanics is strongly model dependent, we decided to choose a representative model ($\lambda_0 = \mu_0 = \tau_0 = 1$) in the subsequent development as a means of exploring general trends. Figures 5–8 aim to investigate the influence of surface mechanics on samples of different sizes, when both the void radius to half-thickness ratio and eccentricity are kept constant. As expected, in the absence of surface mechanics, stress distributions are independent of model sizes and are solely functions of ratios among characteristic lengths, i.e., a/d and c/d. This is not the case, however, when the nominal model of surface mechanics is incorporated. From Figures 5–8, it is clear that the
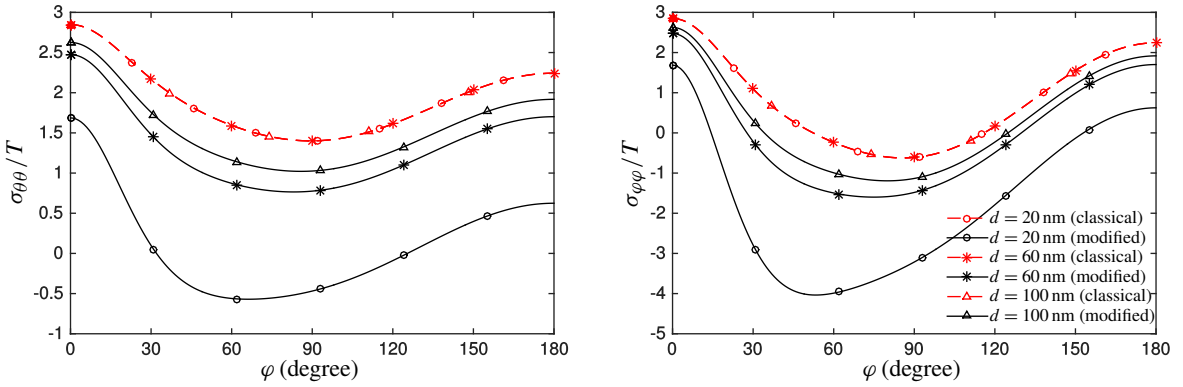
Figure 5. Distribution of hoop, left, and tangential stresses, right, along the void surface ($R = a$). The remaining adjustable parameters are set to: $a = 0.3d$, $c = 0.6d$, and $\lambda_0 = \mu_0 = \tau_0 = 1$ for nonclassical cases.
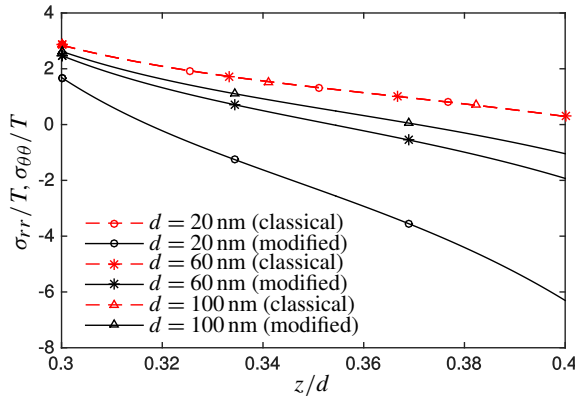

Figure 6. Variation of σ_{rr} and $\sigma_{\theta\theta}$ along the axis of symmetry ($a \leq z \leq d - c$) as a function of nondimensionalized coordinate z/d. The remaining adjustable parameters are set to: $a = 0.3d$, $c = 0.6d$, and $\lambda_0 = \mu_0 = \tau_0 = 1$ for nonclassical cases.

strength of surface mechanics decays monotonically with the model size d. The smaller the model size, the more significant the difference between the classical and modified solutions becomes.

Similar to Figures 3 and 4, Figures 5 and 6 also show the stress concentrations along the void surface and the positive z-axis, respectively. In the latter case ($\varphi = 0$), cylindrical and spherical stresses are connected: $\sigma_{rr} = \sigma_{\varphi\varphi}$ and $\sigma_{zz} = \sigma_{RR}$. Again, the strength of surface mechanics can be qualitatively analyzed by the solution due to a nanovoid embedded in an infinite matrix:

$$(\sigma_{rr}/T)_{\varphi=0} = (\sigma_{\theta\theta}/T)_{\varphi=0} = -\frac{\tau_0}{Ta}\frac{a^3}{R^3} + 1 - \frac{(1-5\nu)}{(7-5\nu)}\frac{a^3}{R^3} + \frac{6}{(7-5\nu)}\frac{a^5}{R^5}. \tag{34}$$

As before, in the above equation the contribution due to surface elasticity has been neglected because of its secondary importance.
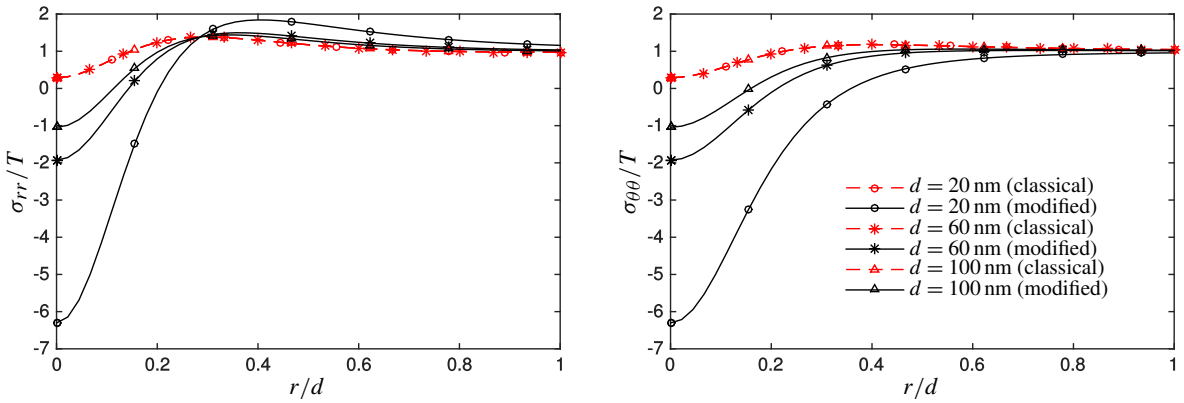
Figure 7. Variation of radial, left, and hoop stresses, right, along the top boundary ($z = d - c$) as a function of nondimensionalized radial coordinate r/d. The remaining adjustable parameters are set to: $a = 0.3d$, $c = 0.6d$, and $\lambda_0 = \mu_0 = \tau_0 = 1$ for nonclassical cases.

Figure 7 shows variations of the radial and hoop stresses on the upper surface of the infinite strip. For all three model sizes, the void surface effects resulted in compressive stress states in the central region of the upper boundary. The compressive domain decreases with model size. Due to symmetry, the maximum compressive stress always occurs at the center $\bar{O}$ of the upper boundary. The discrepancies among the classical and modified solutions are confined to only a few times the radius of the void. This is because the void defect itself is a short-range force field.

Stress distributions on the x-y plane as a function of the model size were also investigated, as shown in Figure 8. The influence of surface mechanics behaves again as a monotonic function. It is interesting to observe that high tensile normal stresses develop on and near the void surface (Figure 8a). In particular, the normal stress σ_{RR} at the free surface of the void becomes nonzero due to the inclusion of surface effects. By the essence of surface mechanics, this stress is equilibrated by the surface divergence of the surface stress ($-2\tau_0/a$). In contrast, low tensile or even compressive $\sigma_{\theta\theta}$ and $\sigma_{\varphi\varphi}$ are produced near the void, representing a relieved stress state. It is no surprise to find that all stresses converge to their far-field counterparts in regions $R \geq 3a$. Once again, the qualitative behavior of the above analysis can be accurately predicted by the closed-form approximations

$$
\begin{aligned}
(\sigma_{RR}/T)_{\varphi=\pi/2} &= \frac{2\tau_0}{Ta}\frac{a^3}{R^3} + 1 - \frac{(13-5\nu)}{(7-5\nu)}\frac{a^3}{R^3} + \frac{6}{(7-5\nu)}\frac{a^5}{R^5}, \\
(\sigma_{\theta\theta}/T)_{\varphi=\pi/2} &= -\frac{\tau_0}{Ta}\frac{a^3}{R^3} + 1 + \frac{(13-20\nu)}{2(7-5\nu)}\frac{a^3}{R^3} - \frac{3}{2(7-5\nu)}\frac{a^5}{R^5}, \\
(\sigma_{\varphi\varphi}/T)_{\varphi=\pi/2} &= -\frac{\tau_0}{Ta}\frac{a^3}{R^3} + \frac{3}{2(7-5\nu)}\frac{a^3}{R^3} - \frac{9}{2(7-5\nu)}\frac{a^5}{R^5}.
\end{aligned}
\tag{35}
$$

Recall that both surface elasticity and the plane boundaries have been ignored in the above equations.

3.4. *Effects of void size.* Three cases of different void radii were examined, when both the strip half-thickness ($d = 20$ nm) and eccentricity ($c = 6$ nm) were fixed. This is a typical parametric study that
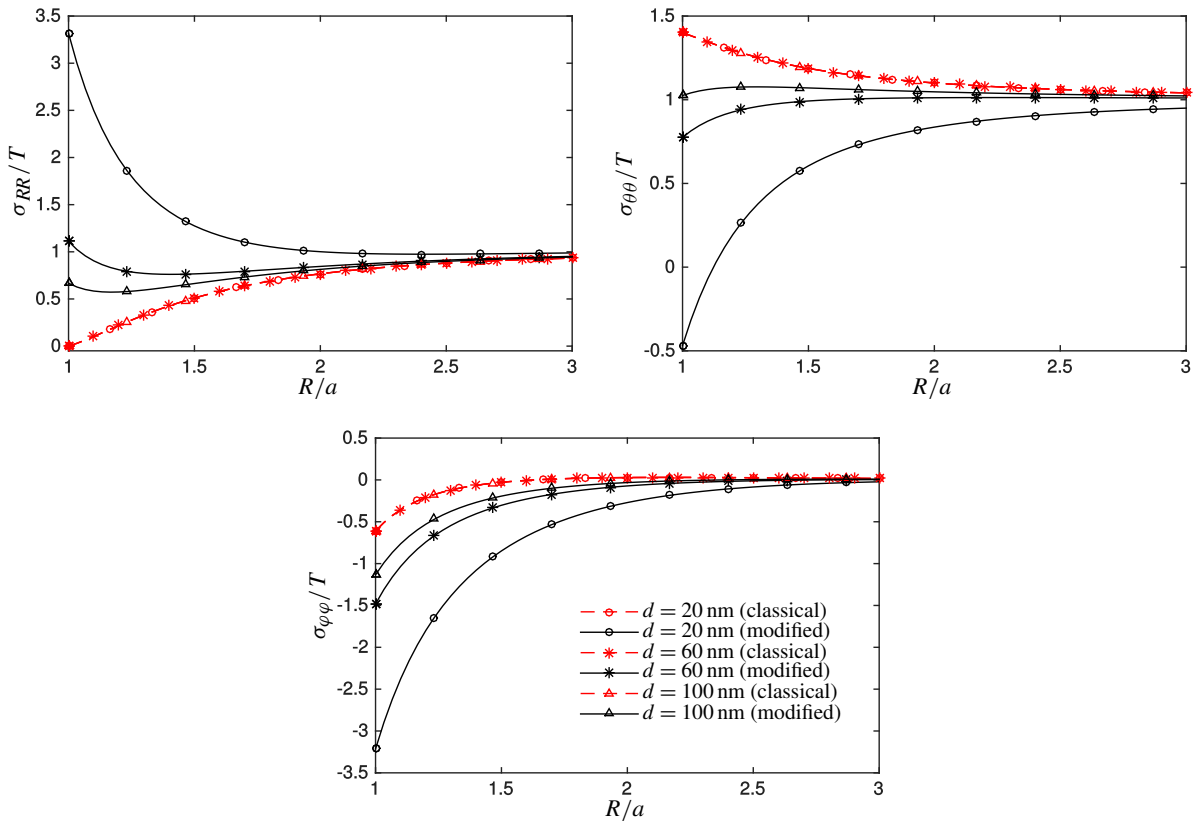
Figure 8. Variation of radial, left; hoop, right; and tangential stresses, bottom, as a function of nondimensionalized radial coordinate R/a. The polar coordinate is kept constant: $\varphi = 90°$. The remaining adjustable parameters are set to: $a = 0.3d$, $c = 0.6d$, and $\lambda_0 = \mu_0 = \tau_0 = 1$ for nonclassical cases.

was performed for a nanovoid embedded in an infinite domain [He and Li 2006; Mi and Kouris 2014]. Emphasis was given to the stress concentrations along the void surface. The hoop ($\sigma_{\theta\theta}$) and tangential ($\sigma_{\varphi\varphi}$) stresses for nanovoids of radius $a = 3$, 6, and 9 nm are shown in Figure 9. The three classical curves vary from one to another due to the presence of eccentricity. The stress distributions are almost symmetric about the x-y plane for the case of $a = 3$ nm. For larger voids, asymmetry in both stress components becomes obvious. The dependence of stress concentration factors on surface effects is quite clear and is as expected. The smaller the nanovoid, the more pronounced the surface effects become. Benefiting from the positive residual surface stress ($\tau_0 = 1$ nm) in the selected nominal model, improvements in stress concentrations were observed in all three cases.

3.5. *Effects of eccentricity.* The last numerical experiment we performed focuses on the influence of eccentricity. Figure 10 illustrates stress concentrations along the surface of a void of radius $a = 6$ nm. Three eccentricities, i.e., $c = 0$, 6, and 12 nm, were considered. For all cases, high tensile values of stress concentration factors were found at the two poles of the void. Low tensile/compressive values
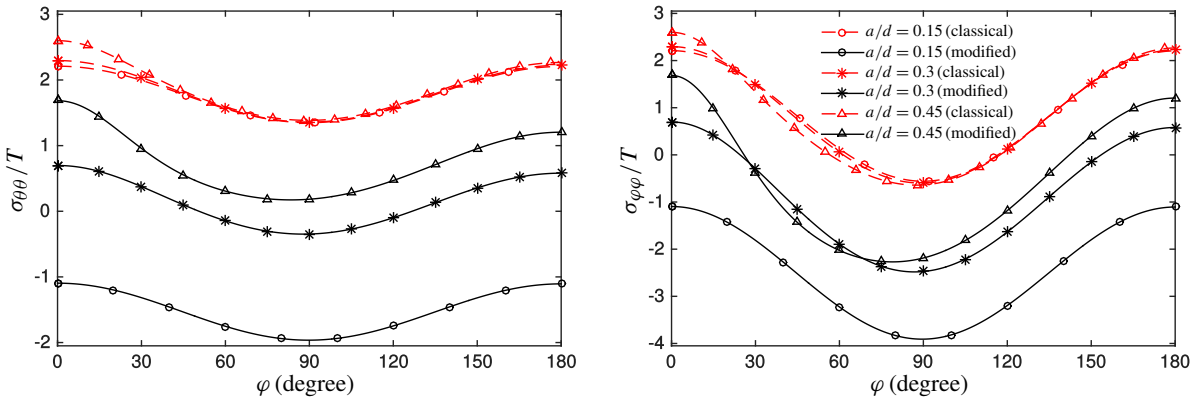
Figure 9. Distribution of hoop, left, and tangential stresses, right, along the void surface ($R = a$). The remaining adjustable parameters are taken to be: $d = 20\,\text{nm}$, $c = 0.3d$, and $\lambda_0 = \mu_0 = \tau_0 = 1$ for nonclassical cases.
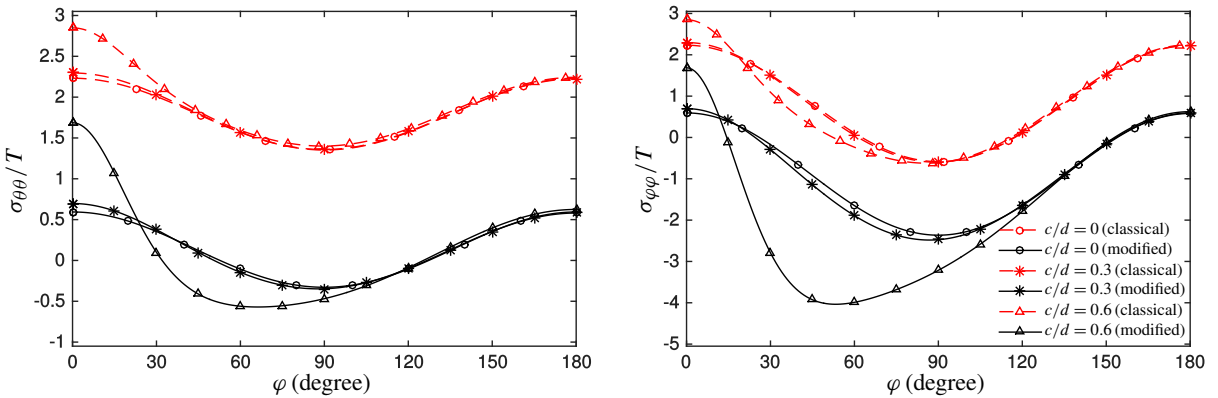

Figure 10. Distribution of hoop, left, and tangential, right, stresses along the void surface ($R = a$). The remaining adjustable parameters are assumed to be: $d = 20\,\text{nm}$, $a = 0.3d$, and $\lambda_0 = \mu_0 = \tau_0 = 1$ for nonclassical cases.

occur near (but not on) the equator of the void, approaching from the north hemisphere. The dependence of stress distributions on the degree of eccentricity is very clear.

As expected, complete symmetry in stress distributions was found for the case of $c = 0$. Due also to the small ratio of void radius to half-thickness ($a/d = 0.3$), both the classical and modified solutions for this case can be reasonably approximated by those due to an infinite substrate. For example, the stress concentration factors at the poles are very close to $\sigma_{\theta\theta/T} = \sigma_{\varphi\varphi}/T = -\tau_0/Ta + 12/(7 - 5\nu)$. Those on the equator of the void surface are well approximated by $\sigma_{\theta\theta}/T = -\tau_0/Ta + 3(4 - 5\nu)/(7 - 5\nu)$ and $\sigma_{\varphi\varphi}/T = -\tau_0/Ta - 3/(7 - 5\nu)$, respectively. For cases with nonzero eccentricities, however, stress distributions on the north hemisphere are significantly disturbed. The disturbance is much less pronounced on the south hemisphere, as can be seen from Figure 10.

4. Concluding remarks

Within the framework of Gurtin and Murdoch's continuum model of surface mechanics, we successfully developed a semianalytical solution, in the forms of infinite series and improper integrals, to the stress concentration problem of a nanosized void embedded in an infinite strip. All-around tensile loads applied at infinity were considered. The method of displacement functions was employed to explore displacements and stresses as functions of void surface material properties, model size, void radius, and eccentricity. The major challenge of the proposed method lies in the evaluation of a number of integrals of Howland type, particularly of those involving Bessel functions. Following extensive numerical experiments, a few observations and conclusions can be summarized:

- Stress distributions were found to depend strongly on the combination of surface material properties. Dimension analysis suggests that for a metallic system the residual surface stress τ_0 is far more crucial than the surface Lamé constants. Positive τ_0 helps to reduce the stress concentration whereas negative values worsen the situation.

- The effects of void surface mechanics are important only for those models whose characteristic lengths are less than 100 nm. Beyond this scale, the void radius to half-thickness ratio (a/d) and relative eccentricity (c/d) govern the strength of stress concentrations.

- Not surprisingly, the impact of void surface mechanics on stress concentrations is in inverse proportion to void radius. For reasonably small ratios a/d, stress distributions degenerate to those of a nanovoid embedded in an infinite medium.

- Eccentricity plays an indispensable role in the determination of stress distributions. As the void approaches the upper boundary, stress concentration factors at the north pole of the void become unbounded for both the classical and modified solutions.

Appendix A: Evaluation of integrals of Howland type

To perform numerical experiments, the integrals defined in (31) must be evaluated. The integrals $I_n^{\pm}$ and $L_n^{\pm}$ have previously been computed [Ling and Lin 1971; Ling 1978] to 25 significant figures. It is worth noticing that as n approaches infinity, I_n^+ and L_n^+ tend to 2 and $\frac{1}{2}^k$, respectively. On the other hand, both I_n^- and L_n^- tend to zero.

Now, let us expand $\sinh[2cx/d]$ into the power series of its argument; the integrals $J_n^{\pm}$ then become

$$J_n^{\pm} = \sum_{m=0}^{\infty} \left(\frac{c}{d}\right)^{2m+1} \frac{(n+2m+1)!}{n!(2m+1)!} I_{n+2m+1}^{\pm}.$$

Since I_n^+ tends to 2 as the integer n tends to infinity, J_n^+ is a slowly convergent series. In order to improve the convergence, a Kummer transformation may be enforced [Ling 1957]:

$$J_n^+ = \frac{\{(1+c/d)^{n+1} - (1-c/d)^{n+1}\}}{(1-c^2/d^2)^{n+1}} + \sum_{m=0}^{\infty} \left(\frac{c}{d}\right)^{2m+1} \frac{(n+2m+1)!}{n!(2m+1)!} (I_{n+2m+1}^+ - 2).$$

In contrast, the series J_n^- converges rapidly to zero with increasing n. Following the same strategy, the integrals $K_n^\pm$ can be evaluated as

$$K_n^+ = \frac{\{(1+c/d)^{n+1}+(1-c/d)^{n+1}\}}{(1-c^2/d^2)^{n+1}} + \sum_{m=0}^{\infty}\left(\frac{c}{d}\right)^{2m}\frac{(n+2m)!}{n!(2m)!}(I_{n+2m}^+ - 2),$$

$$K_n^- = \sum_{m=0}^{\infty}\left(\frac{c}{d}\right)^{2m}\frac{(n+2m)!}{n!(2m)!}I_{n+2m}^-.$$

Benefiting from the rapid convergence of both L_n^+ and L_n^-, series expansions of the hyperbolic sine and cosine functions are sufficient for evaluating the integrals $M_n^\pm$ and $N_n^\pm$:

$$M_n^\pm = \sum_{m=0}^{\infty}\left(\frac{c}{d}\right)^{2m+1}\frac{(n+2m+1)!}{n!(2m+1)!}L_{n+2m+1}^\pm, \qquad N_n^\pm = \sum_{m=0}^{\infty}\left(\frac{c}{d}\right)^{2m}\frac{(n+2m)!}{n!(2m)!}L_{n+2m}^\pm.$$

Appendix B: Expressions of dimensionless functions defined in (32)

$$i_{A1} = (n+1)(n+2), \quad i_{B1} = \frac{n(n^2+3n-2\nu)}{(2n-1)}, \quad i_{B2} = \frac{(n+1)(n+2)(n+5-4\nu)}{(2n+3)},$$

$$i_{SA1} = \frac{(n+1)(n+2)(2\lambda_0+2\mu_0+(n+1)\tau_0)}{2aG}\frac{d^{n+3}}{a^{n+3}},$$

$$i_{SB2} = \frac{(n+1)(n+2)(n+5-4\nu)(2\lambda_0+2\mu_0+(n+1)\tau_0)}{2aG(2n+3)}\frac{d^{n+3}}{a^{n+3}},$$

$$i_{SB1} = \frac{n\{(n^2-n(1-4\nu)+2-4\nu)(2\lambda_0+2\mu_0)+(n^3+n^2(6-4\nu)-n(1-4\nu)-2)\tau_0\}}{2aG(2n-1)}\frac{d^{n+1}}{a^{n+1}},$$

$$l_{A1} = (n+2), \quad l_{B1} = \frac{(n^2-2+2\nu)}{(2n-1)}, \quad l_{B2} = \frac{(n+2)(n+5-4\nu)}{(2n+3)},$$

$$l_{SA1} = \frac{(n+2)((n+1)\lambda_0+2n\mu_0+2\tau_0)}{2aG}\frac{d^{n+3}}{a^{n+3}},$$

$$l_{SB2} = \frac{(n+2)(n+5-4\nu)((n+1)\lambda_0+2n\mu_0+2\tau_0)}{2aG(2n+3)}\frac{d^{n+3}}{a^{n+3}},$$

$$l_{SB1} = \frac{\{n(n^2-n(1-4\nu)+2-4\nu)\lambda_0+2(n^3-n^2(2-4\nu)-2n+4-4\nu)\mu_0+2(n^2+4(n-1)(1-\nu))\tau_0\}}{2aG(2n-1)}\frac{d^{n+1}}{a^{n+1}},$$

$$i_{\alpha1} = n(n-1), \quad i_{\beta1} = \frac{n(n-1)(n-4+4\nu)}{(2n-1)}, \quad i_{\beta2} = \frac{(n+1)(n^2-n-2-2\nu)}{(2n+3)},$$

$$i_{S\alpha1} = \frac{n(n-1)(2\lambda_0+2\mu_0-n\tau_0)}{2aG}\frac{a^{n-2}}{d^{n-2}},$$

$$i_{S\beta1} = \frac{n(n-1)(n-4+4\nu)(2\lambda_0+2\mu_0-n\tau_0)}{2aG(2n-1)}\frac{a^{n-2}}{d^{n-2}},$$

$$i_{S\beta2} = \frac{(n+1)\{(n^2+n(3-4\nu)+4-8\nu)(2\lambda_0+2\mu_0)-(n^3-n^2(3-4\nu)-2n(5-6\nu)-4+8\nu)\tau_0\}}{2aG(2n+3)}\frac{a^n}{d^n},$$

$$l_{\alpha 1} = -(n-1), \quad l_{\beta 1} = -\frac{(n-1)(n-4+4\nu)}{(2n-1)}, \quad l_{\beta 2} = -\frac{(n^2+2n-1+2\nu)}{(2n+3)},$$

$$l_{S\alpha 1} = \frac{(n-1)(n\lambda_0 + 2(n+1)\mu_0 - 2\tau_0)}{2aG} \frac{a^{n-2}}{d^{n-2}},$$

$$l_{S\beta 1} = \frac{(n-1)(n-4+4\nu)(n\lambda_0 + 2(n+1)\mu_0 - 2\tau_0)}{2aG(2n-1)} \frac{a^{n-2}}{d^{n-2}},$$

$$l_{S\beta 2} = \frac{\left\{(n+1)(n^2+n(3-4\nu)+4-8\nu)\lambda_0 + 2\left(n^3+n^2(5-4\nu)+n(5-8\nu)-3\right)\mu_0 \atop \qquad\qquad\qquad\qquad - 2(n^2-n(2-4\nu)-7+8\nu)\tau_0\right\}}{2aG(2n+3)} \frac{a^n}{d^n}.$$

Appendix C: Evaluation of integrals of Howland type involving a Bessel function

The 24 integrals that were encountered when evaluating stresses in cylindrical coordinates from (13) and (14) are as follows:

$$\left\{ {IS_{m,n}^{\pm} \atop IC_{m,n}^{\pm}} \right\} = \frac{1}{n!} \int_0^{\infty} \left\{ {\sinh[zx/d] \atop \cosh[zx/d]} \right\} I^{\pm} x^n J_m[rx/d] \, dx,$$

$$\left\{ {JS_{m,n}^{\pm} \atop JC_{m,n}^{\pm}} \right\} = \frac{1}{n!} \int_0^{\infty} \left\{ {\sinh[zx/d] \atop \cosh[zx/d]} \right\} I^{\pm} x^n \sinh[2cx/d] J_m[rx/d] \, dx,$$

$$\left\{ {KS_{m,n}^{\pm} \atop KC_{m,n}^{\pm}} \right\} = \frac{1}{n!} \int_0^{\infty} \left\{ {\sinh[zx/d] \atop \cosh[zx/d]} \right\} I^{\pm} x^n \cosh[2cx/d] J_m[rx/d] \, dx,$$

$$\left\{ {LS_{m,n}^{\pm} \atop LC_{m,n}^{\pm}} \right\} = \frac{1}{n!} \int_0^{\infty} \left\{ {\sinh[zx/d] \atop \cosh[zx/d]} \right\} I^{\pm} e^{-2x} x^n J_m[rx/d] \, dx,$$

$$\left\{ {MS_{m,n}^{\pm} \atop MC_{m,n}^{\pm}} \right\} = \frac{1}{n!} \int_0^{\infty} \left\{ {\sinh[zx/d] \atop \cosh[zx/d]} \right\} I^{\pm} e^{-2x} x^n \sinh[2cx/d] J_m[rx/d] \, dx,$$

$$\left\{ {NS_{m,n}^{\pm} \atop NC_{m,n}^{\pm}} \right\} = \frac{1}{n!} \int_0^{\infty} \left\{ {\sinh[zx/d] \atop \cosh[zx/d]} \right\} I^{\pm} e^{-2x} x^n \cosh[2cx/d] J_m[rx/d] \, dx.$$

Take the first group of the above integrals as an example. Consider the auxiliary integrals

$$\bar{I}_{m,n}^{\pm} = \frac{1}{n!} \int_0^{\infty} I^{\pm} x^n J_m[rx/d] \, dx.$$

Following [Ling and Wu 1982], we replace the Bessel function by its usual series representation and integrate:

$$\bar{I}_{m,n}^{\pm} = \sum_{k=0}^{\infty} \frac{(-1)^k (n+m+2k)!}{n!k!(m+k)!2^n} \left(\frac{r}{4d}\right)^{m+2k} I_{n+m+2k}^{\pm}.$$

Since the limit of I_n^+ is 2 as n tends to infinity, the convergence of $\bar{I}_{m,n}^+$ may again be improved by the use of a Kummer transformation. Finally, the first group of the 24 integrals can be evaluated in terms of

the auxiliary integrals

$$IS_{m,n}^{\pm} = \sum_{k=0}^{\infty} \frac{(n+2k+1)!}{n!(2k+1)!}\left(\frac{z}{d}\right)^{2k+1} \bar{I}_{m,n+2k+1}^{\pm}, \quad IC_{m,n}^{\pm} = \sum_{k=0}^{\infty} \frac{(n+2k)!}{n!(2k)!}\left(\frac{z}{d}\right)^{2k} \bar{I}_{m,n+2k}^{\pm}.$$

Although tedious, the remaining integrals can be evaluated in a procedure similar to the one described above.

Acknowledgements

References

[Arfken et al. 2013] G. B. Arfken, H. J. Weber, and F. E. Harris, *Mathematical methods for physicists: a comprehensive guide*, 7th ed., Elsevier, Amsterdam, 2013.

[Barber 2010] J. R. Barber, *Elasticity*, 3rd ed., Springer, New York, 2010.

[Benveniste 2006] Y. Benveniste, "A general interface model for a three-dimensional curved thin anisotropic interphase between two anisotropic media", *J. Mech. Phys. Solids* **54**:4 (2006), 708–734.

[Boccardo et al. 2015] V. Boccardo, E. Godoy, and M. Durán, "An efficient semi-analytical method to compute displacements and stresses in an elastic half-space with a hemispherical pit", *Adv. Appl. Math. Mech.* **7**:3 (2015), 295–322.

[Cammarata 1994] R. C. Cammarata, "Surface and interface stress effects in thin films", *Prog. Surf. Sci* **46**:1 (1994), 1–38.

[Chen and Yao 2014] S. Chen and Y. Yao, "Elastic theory of nanomaterials based on surface-energy density", *J. Appl. Mech. (ASME)* **81**:12 (2014), art. id. 121002, 12 pp.

[Duan et al. 2009] H. L. Duan, J. Wang, and B. Karihaloo, "Theory of elasticity at the nanoscale", *Adv. Appl. Mech.* **42** (2009), 1–68.

[Gradshteyn and Ryzhik 2014] I. S. Gradshteyn and I. M. Ryzhik, *Table of integrals, series, and products*, 8th ed., Elsevier, Boston, Massachusetts, 2014.

[Gumbsch and Daw 1991] P. Gumbsch and M. S. Daw, "Interface stresses and their effects on the elastic moduli of metallic multilayers", *Phys. Rev. B* **44** (1991), 3934–3938.

[Gurtin and Murdoch 1975] M. E. Gurtin and I. A. Murdoch, "A continuum theory of elastic material surfaces", *Arch. Ration. Mech. Anal.* **57**:4 (1975), 291–323. Correction in **59**:4 (1975), 389–390.

[Gurtin and Murdoch 1978] M. E. Gurtin and A. I. Murdoch, "Surface stress in solids", *Int. J. Solids Struct.* **14**:6 (1978), 431–440.

[He and Li 2006] L. H. He and Z. R. Li, "Impact of surface stress on stress concentration", *Int. J. Solids Struct.* **43**:20 (2006), 6208–6219.

[Huang and Wang 2013] Z. Huang and J. Wang, "Micromechanics of nanocomposites with interface energy effect", pp. 303–348 in *Handbook of micromechanics and nanomechanics*, edited by S. Li and X.-L. Gao, CRC Press, Boca Raton, FL, 2013.

[Li et al. 2006] Z. R. Li, C. W. Lim, and L. H. He, "Stress concentration around a nano-scale spherical cavity in elastic media: effect of surface stress", *Eur. J. Mech. A Solids* **25**:2 (2006), 260–270.

[Ling 1957] C.-B. Ling, "Tables of values of 16 integrals of algebraic-hyperbolic type", *Math. Tables Aids Comput.* **11** (1957), 160–166.

[Ling 1978] C.-B. Ling, "Further evaluation of Howland integrals", *Math. Comput.* **32** (1978), 900–904.

[Ling and Lin 1971] C.-B. Ling and J. Lin, "A new method of evaluation of Howland integrals", *Math. Comput.* **25** (1971), 331–337.

[Ling and Wu 1982] C.-B. Ling and M.-J. Wu, "Evaluation of integrals of Howland type involving a Bessel function", *Math. Comput.* **38** (1982), 215–222.

[Mi and Kouris 2006] C. Mi and D. Kouris, "Nanoparticles under the influence of surface/interface elasticity", *J. Mech. Mater. Struct.* **1**:4 (2006), 763–791.

[Mi and Kouris 2013] C. Mi and D. Kouris, "Stress concentration around a nanovoid near the surface of an elastic half-space", *Int. J. Solids Struct.* **50**:18 (2013), 2737–2748.

[Mi and Kouris 2014] C. Mi and D. Kouris, "On the significance of coherent interface effects for embedded nanoparticles", *Math. Mech. Solids* **19**:4 (2014), 350–368.

[Mi and Kouris 2015] C. Mi and D. Kouris, "Surface mechanics implications for a nanovoided metallic thin-plate under uniform boundary loading", *Math. Mech. Solids* (2015), art. id. 1081286515595262, 19 pp.

[Mi et al. 2008] C. Mi, S. Jun, D. A. Kouris, and S. Y. Kim, "Atomistic calculations of interface elastic properties in noncoherent metallic bilayers", *Phys. Rev. B* **77** (2008), art. id. 075425, 12 pp.

[Mi et al. 2016] C. Mi, Z. Sun, and D. Kouris, "The hemispherical nanopit at the plane boundary of an elastic half-space subjected to statically equivalent shear tractions", *J. Mech. Mater. Struct.* **11**:5 (2016), 595–614.

[Mura 1987] T. Mura, *Micromechanics of defects in solids*, Martinus Nijhoff, Boston, 1987.

[Sharma and Ganti 2004] P. Sharma and S. Ganti, "Size-dependent Eshelby's tensor for embedded nano-inclusions incorporating surface/interface energies", *J. Appl. Mech.* (*ASME*) **71**:5 (2004), 663–671.

[Shenoy 2005] V. B. Shenoy, "Atomistic calculations of elastic properties of metallic fcc crystal surfaces", *Phys. Rev. B* **71** (2005), art. id. 094104, 11 pp.

[Springholz et al. 1998] G. Springholz, V. Holy, M. Pinczolits, and G. Bauer, "Self-organized growth of three-dimensional quantum-dot crystals with fcc-like stacking and a tunable lattice constant", *Science* **282**:5389 (1998), 734–737.

[Tsuchida and Nakahara 1970] E. Tsuchida and I. Nakahara, "Three-dimentsional stress concentration around a spherical cavity in a semi-infinite elastic body", *Bull. Jpn. Soc. Mech. Eng.* **13**:58 (1970), 499–508.

[Tsuchida and Nakahara 1972] E. Tsuchida and I. Nakahara, "Stresses in a semi-infinite body subjected to uniform pressure on the surface of a cavity and the plane boundary", *Bull. Jpn. Soc. Mech. Eng.* **15**:79 (1972), 1–10.

[Tsuchida and Nakahara 1974] E. Tsuchida and I. Nakahara, "Stress concentration around a spherical cavity in a semi-infinite elastic body under uniaxial tension", *Bull. Jpn. Soc. Mech. Eng.* **17**:112 (1974), 1207–1217.

[Tsuchida and Nakahara 1976] E. Tsuchida and I. Nakahara, "Three-dimensional stress concentration around a spherical cavity in a thick plate under uniaxial tension", *Bull. Jpn. Soc. Mech. Eng.* **19**:136 (1976), 1107–1114.

[Tsuchida et al. 1976] E. Tsuchida, S. Togawa, I. Nakahara, and M. Kodama, "Stresses in a thick plate containing an eccentric spherical cavity under uniaxial tension", *Bull. Jpn. Soc. Mech. Eng.* **19**:134 (1976), 838–848.

[Wang et al. 2011] J. Wang, Z. Huang, H. Duan, S. Yu, X. Feng, G. Wang, W. Zhang, and T. Wang, "Surface stress effect in mechanics of nanostructured materials", *Acta Mech. Solida Sin.* **24**:1 (2011), 52–82.

CHANGWEN MI: mi@seu.edu.cn
Jiangsu Key Laboratory of Engineering Mechanics, School of Civil Engineering, Southeast University, 2 Sipailou Street, Nanjing, 210096, China

JOURNAL OF MECHANICS OF MATERIALS AND STRUCTURES

msp.org/jomms

Founded by Charles R. Steele and Marie-Louise Steele

Journal of Mechanics of Materials and Structures